Journal of
Materials Chemistry C

COMMUNICATION

View Article Online
View Journal | View Issue

Cite this: J. Mater. Chem. C, 2015, 3, 11286

Received 6th August 2015,
Accepted 12th October 2015

DOI: 10.1039/c5tc02447a

www.rsc.org/MaterialsC

Highly luminescent perovskite–aluminum oxide composites†

Giulia Longo, Antonio Pertegás, Laura Martínez-Sarti, Michele Sessolo* and Henk J. Bolink

In this communication we report on the preparation of $CH_3NH_3PbBr_3$ perovskite/Al_2O_3 nanoparticle composites in a thin film configuration and demonstrate their high photoluminescence quantum yield. The composite material is solution-processed at low temperature, using stable alumina nanoparticle dispersions. There is a large influence of the alumina nanoparticle concentration on the perovskite morphology and on its photoluminescence.

Recently, organic–inorganic (hybrid) metal halide perovskites have become the focus of renewed interest thanks to their remarkable performances in photovoltaics, as increasing power conversion efficiencies, now exceeding 20%, are being reported.[1–6] The most studied compound in photovoltaics is the methylammonium lead iodide $CH_3NH_3PbI_3$ perovskite, due to its strong bandgap absorption at about 1.6 eV. One of the interesting features of this class of semiconductors is that their optical properties can be modulated by simple substitution of their constituents.[7] The correspondent bromide compound $CH_3NH_3PbBr_3$ has a bandgap of about 2.3 eV, making it a good candidate for visible lasing and light-emission applications.[8,9] For both applications, the active material should show high photoluminescence quantum yield (PLQY), in order to efficiently convert the generated (either electrically or optically) charges into photons. Unfortunately, the photoluminescence (PL) of hybrid perovskites depends on the excitation intensity, being high at very high excitation intensity while very low when the excitation intensity decreases.[10] In electroluminescence, this means that high current densities are needed in order to produce significant light emission, which leads to a low power conversion efficiency of the devices.[8,11] A promising approach to reduce the non-radiative recombination in hybrid perovskites is the synthesis of nanoparticles. This has led to materials that show substantially enhanced photoluminescence, reaching PLQYs exceeding 90%.[12–15] The nanoparticle preparation, however, relies on complex chemical synthesis which might undermine the scalability of this approach. Moreover, the PLQY tends to substantially reduce when nanocrystals are processed as thin films, due to spontaneous aggregation of the perovskite.[16] It has also been shown how enhanced photoluminescence can be obtained by impregnation of a pre-formed mesoporous inorganic matrix (such as alumina) with the perovskite precursor solution, albeit a quantitative estimation of the PLQY has not been reported.[17,18] From a film forming/processing perspective, a more appealing approach is the deposition of composite films from blends of polymer or low molecular weight organic semiconductors, resulting in the formation of nano-/micro-domains of hybrid perovskites.[19,20] Here we present a hybrid approach for the preparation of high PLQY perovskite-based materials, which consists in the processing of blends of the perovskite precursor with stable alumina nanoparticle (NP) suspensions. Thin films were deposited at low temperature from solution, and a PLQY of up to 39% in the solid state was obtained. We show that the self-assembly of the alumina NPs constrains the growth of the perovskite to the nanoscale, resulting in the spontaneous formation of isotropic $CH_3NH_3PbBr_3$ nanocrystals.

The perovskite precursor solution was prepared by mixing $PbBr_2$ and CH_3NH_3Br in DMF in a 1 : 3 molar ratio. Subsequently, an aqueous dispersion of Al_2O_3 NPs with an average size of 10 nm was added to the perovskite precursor. Different amounts of Al_2O_3 NPs were used to evaluate the effect of the perovskite/NP ratio on the optical properties of the composite. Thin films of the composite materials were obtained by spin-coating the solution on glass or quartz substrates in air, followed by annealing on a hot plate at 90 °C for 1 hour. Processing of the composite films in air was possible due to their good stability to moisture. The origin of the relative moisture-insensitivity of $CH_3NH_3PbBr_3$:Al_2O_3 NP systems is not completely understood. In these films, however, most of the perovskite is surrounded by aluminum oxide, which is known to retard the degradation of hybrid perovskites.[21] On the other hand, pure $CH_3NH_3PbBr_3$ perovskite films were deposited and annealed in a nitrogen-filled glovebox, due to the limited stability of the compound in air.

Instituto de Ciencia Molecular (ICMOL), Universidad de Valencia, 46980 Paterna, Spain. E-mail: michele.sessolo@uv.es

† Electronic supplementary information (ESI) available: UV-Vis optical absorption of perovskite/Al_2O_3 NP films with high NP content (75 wt%). See DOI: 10.1039/c5tc02447a

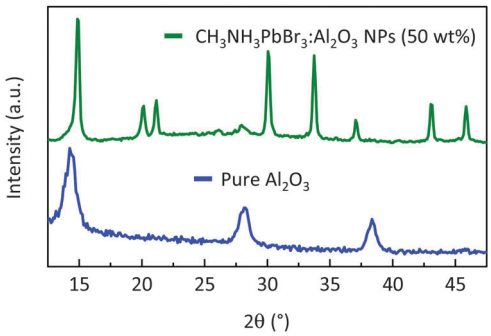

Fig. 1 GIXRD spectra of a mixed $CH_3NH_3PbBr_3/Al_2O_3$ thin film compared to the reference obtained from a pure Al_2O_3 NP layer.

The formation of crystalline perovskite was confirmed by grazing incidence X-ray diffraction (GIXRD) of the obtained thin films. In Fig. 1, the diffraction spectra of a composite film containing 50 wt% of alumina NPs are depicted. The spectra showed the diffraction pattern expected for $CH_3NH_3PbBr_3$, confirming the formation of the perovskite in the presence of a high concentration of alumina NPs.[22] The peak at 20.1° indicates that a small amount of the ammonium salt is still present in the composite film (see Fig. S1 in the ESI,† for the reference diffractogram of the pure CH_3NH_3Br and $CH_3NH_3PbBr_3$ compounds).

In Fig. 2a, the UV-Vis absorption spectra of a series of thin films with increasing Al_2O_3 NP content is depicted. The pure perovskite absorption spectra are shown as a reference. We observed that samples with low NP content (30 wt%) are not fully converted to the perovskite structure with this annealing time and temperature, as testified by the spectral feature at ~310 nm which corresponds to lead bromide complexes.[23] By increasing the alumina NP content, the peak at 310 nm fades while the absorption onset at ~525 nm, corresponding to the band-to-band transition of the perovskite, appears. These observations suggest that the presence of alumina NPs favors the perovskite formation. A similar enhanced crystallization has been observed for $CH_3NH_3PbI_3$ in mesoporous scaffolds.[2] Interestingly, perovskite/Al_2O_3 NP films with high NP content (75 wt%) spontaneously form the crystalline perovskite phase even at room temperature (Fig. S2, ESI†).

The photoluminescence characteristics of the Al_2O_3 NP thin films were studied using a Xe lamp coupled to a monochromator as the excitation source and a spectrometer coupled to an integrated sphere (Hamamatsu C9920-02 with a Hamamatsu PMA-11 optical detector) in order to quantitatively determine the PLQY. For the pure perovskite film and for films with a low NP content (<30 wt%), only weak photoluminescence could be observed, with PLQY values within the measurement error of the setup (<2%). This is partially due to the low excitation intensity used in the experiments (<0.4 mW cm^{-2}). On the other hand, with increasing NP loading, the typical green emission of the $CH_3NH_3PbBr_3$ perovskite started to rise (Fig. 2b). A strong dependence of the PLQY on the Al_2O_3 content is apparent which reaches a maximum of 26% for a NP concentration of 50 wt% (Fig. 2c). This PLQY is slightly higher than what was reported for thin films of colloidal $CH_3NH_3PbBr_3$ nanocrystals.[12] This is particularly striking when taking into account the simple material preparation and its processing in air from water-based dispersions. By increasing the annealing time at 90 °C to 3 hours, the PLQY of the $CH_3NH_3PbBr_3$:Al_2O_3 NP (50 wt%) composite thin films is

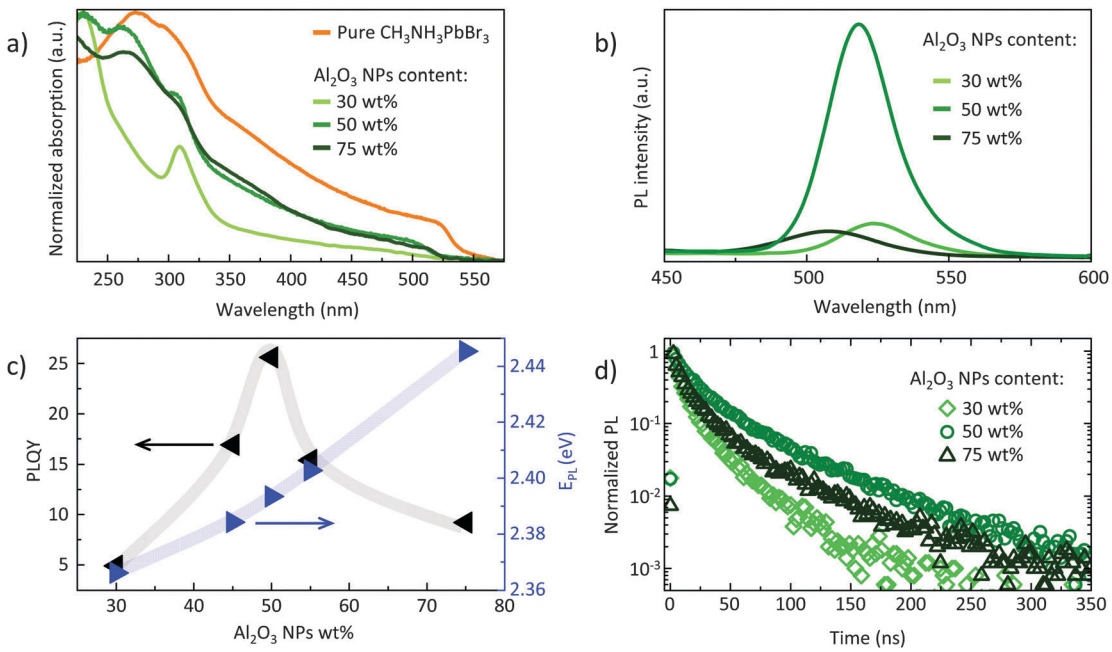

Fig. 2 Photophysical characterization of the composite $CH_3NH_3PbBr_3/Al_2O_3$ NP thin films with increasing NP concentration. (a) Normalized UV-Vis spectra of thin films, with the pure perovskite absorption reported as a reference and (b) correspondent photoluminescence spectra recorded by excitation at 380 nm. (c) Trend of the PLQY (black, left) and of the energy of the PL emission peak (blue, right) *vs.* Al_2O_3 NP loading. The broad lines in (c) are drawn as guide to the eye. (d) Time-resolved PL measurements taken at the peak emission wavelength of each sample, with a pump wavelength of 380 nm.

increased to 39%. Together with the increase in the PLQY with increasing Al_2O_3 NP content, a slight but continuous blue-shift of the emission energy occurs (Fig. 2d). This shift in emission wavelength was also observed in nano-sized $CH_3NH_3PbBr_3$ perovskite blended with organic semiconductors,[19] which was ascribed to quantum confinement effects. From GIXRD line broadening, a crystallite size of about 20 nm for the films containing 30 wt% Al_2O_3 NPs was derived. For such Al_2O_3 NP concentrations, the photoluminescence maxima is 2.37 eV, which agrees well with what reported for similar size perovskites.[19] Even considering the rough estimation of the size by GIXRD, here we tend to exclude quantum confinement effects, since the predicted Bohr radius for $CH_3NH_3PbBr_3$ (2.2 nm) is significantly smaller than the particle dimensions obtained in the Al_2O_3 NP–perovskite composite films.[24] Recently, D'Innocenzo *et al.* observed a similar (in magnitude) blue-shift of the photoluminescence peak when decreasing the crystallite size of $CH_3NH_3PbI_3$ thin films.[25] They associated the measured shift with a distortion of the I–Pb–I bond, which has been theoretically predicted and also experimentally observed by Raman spectroscopy.[26,27] Since such distortion would be especially significant in perovskites grown into a mesoporous scaffold, it might be responsible for the blue shift observed in our $CH_3NH_3PbBr_3/Al_2O_3$ NP blends. In order to gain further insights into the origin of the observed PLQY variation, the time-resolved PL was recorded for the same set of samples (Fig. 2d). We observed very fast PL decays with lifetimes τ_e (the time to reach 1/e of the initial intensity) of 9, 20 and 11 ns for the samples with NP content of 30, 50 and 75 wt%, respectively, in agreement with the presence of nano-sized perovskite crystallites.[25] A longer lifetime was recorded for the sample with higher PLQY (50 wt% NPs), suggesting a reduction of the nonradiative channels at this concentration.

For a structure–property correlation of the photoluminescence observed in the composite thin films, the material morphology was studied by scanning electron microscopy (SEM). The surface images of the samples with 30, 50 and 75 wt% Al_2O_3 NP content are reported in Fig. 3 (a, b, and c, respectively). Interestingly, we observed the presence of relatively large crystals (diameter of 2–4 μm) lying on a smooth surface. The profile of a single crystal was measured by atomic force microscopy (Fig. 3d), and found to protrude about 200 nm above the sample surface. A very similar morphology has been recently reported by Li *et al.* when solution processing films from $CH_3NH_3PbBr_3$ blends with an inert polymer.[20] In our films the system morphology is more complex since the background surface consists of an Al_2O_3 mesoporous scaffold observable at higher magnification (Fig. 3e). The composite material contains a large amount of $CH_3NH_3PbBr_3$ perovskite, as confirmed by energy dispersive X-ray analysis (EDXA, Fig. 3f). With increasing Al_2O_3 NP content, the formation of the crystals seems to be hindered (Fig. S4, ESI†), finally fading into round aggregates at the highest measured concentration (75 wt%, Fig. 3c). The observed perovskite super-structure on the alumina film is substantially different compared to the often referred to "capping layer" in the literature.[28] The capping layer is formed when a pure perovskite precursor solution is cast on top of a pre-formed mesoporous metal oxide film, resulting in excess,

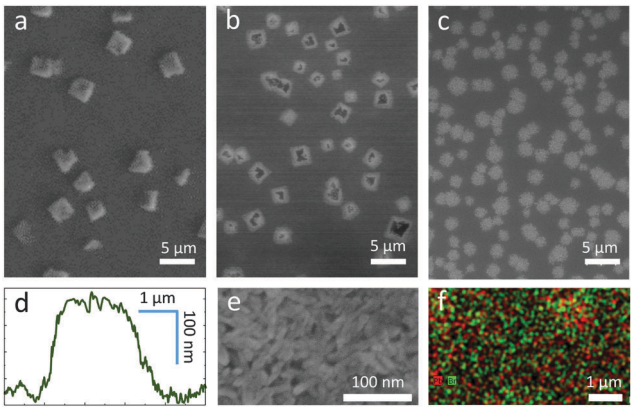

Fig. 3 SEM pictures of the mixed $CH_3NH_3PbBr_3/Al_2O_3$ NP thin films at 30, 50 and 75 wt% Al_2O_3 NP content (a, b, and c, respectively). (d) AFM profile of a single crystal from a sample containing 30 wt% Al_2O_3 NPs. (e) Higher magnification SEM image of the sample surface and (f) correspondent EDXA map for lead (red) and bromide (green).

superficial perovskite growth. While the photoluminescent properties of hybrid perovskites are expected to be morphology-dependent, the large structures observed in SEM images are unlikely the origin of the high photoluminescence observed. The observed blue-shift and the very short PL lifetime are more consistent when originating from perovskite crystals whose size is limited by the alumina NP scaffold. On the other hand, at low alumina concentration (<30 wt%) the perovskite aggregation within the alumina scaffold is obviously favored and this translates into PL quenching. In order to investigate the morphology of the $CH_3NH_3PbBr_3/Al_2O_3$ NP composite, transmission electron microscopy (TEM) was performed on powders obtained from scratched films. The TEM analysis (Fig. 4a) shows a morphology in accordance with that observed by SEM (Fig. 3e), where rod-like Al_2O_3 NPs assemble forming a dense mesoporous layer.

More interesting is the observation of a high concentration of isotropic nanoparticles with a considerably different contrast. The high resolution TEM (HR-TEM, Fig. 4b) shows that the observed

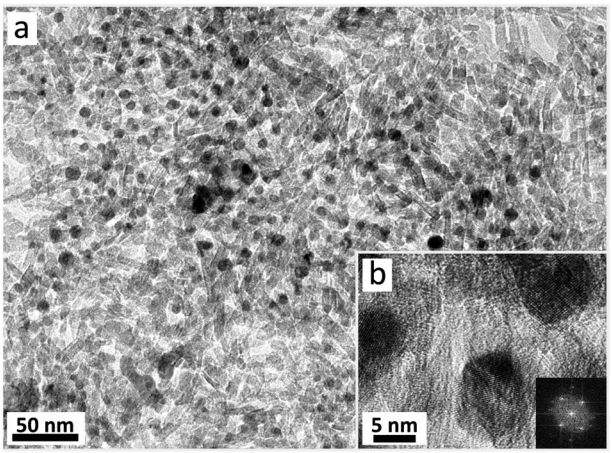

Fig. 4 (a) TEM picture of the mixed $CH_3NH_3PbBr_3/Al_2O_3$ NP thin films at 50 wt% Al_2O_3 NP content at different magnifications. The inset (b) is a HR-TEM image of few isolated NPs with the correspondent FFT.

nanoparticles are highly crystalline, and the fast Fourier transform (FFT) of a single nanocrystal confirms the presence of the cubic phase described for $CH_3NH_3PbBr_3$.[16] The electron microscopy hence confirms the formation of a nanostructured composite material where the growth of the hybrid perovskite is controlled and limited by the presence of the alumina NPs, as postulated by analyzing the photophysical properties.

Conclusions

In summary, high photoluminescence quantum yield $CH_3NH_3PbBr_3$ perovskite/alumina nanoparticle composite materials have been prepared. A strong enhancement of the photoluminescence as a consequence of the formation of perovskite nanocrystals is observed. The nanocrystal dimensions are governed by the size and concentration of the alumina nanoparticles. An optimum photoluminescence was found at 50 wt% of the alumina nanoparticles at which quantum yields up to 40% were recorded in thin solid films. Furthermore, these materials can be easily processed from solution at low temperature in air and are rather moisture insensitive, making them interesting candidates for future light-emitting and lasing applications.

Acknowledgements

This work was supported by the European Union 7th framework program LUMINET (grant 316906), the Spanish Ministry of Economy and Competitiveness (MINECO) (MAT2014-55200) and the Generalitat Valenciana (Prometeo/2012/053). The authors would like to thank Valerio D'Innocenzo for fruitful discussions on the optical lifetime measurements.

Notes and references

1 A. Kojima, K. Teshima, Y. Shirai and T. Miyasaka, *J. Am. Chem. Soc.*, 2009, **131**, 6050–6051.
2 M. M. Lee, J. Teuscher, T. Miyasaka, T. N. Murakami and H. J. Snaith, *Science*, 2012, **338**, 643–647.
3 J. Burschka, N. Pellet, S. J. Moon, R. Humphry-Baker, P. Gao, M. K. Nazeeruddin and M. Grätzel, *Nature*, 2013, **499**, 316–319.
4 N. J. Jeon, J. H. Noh, Y. C. Kim, W. S. Yang, S. Ryu and S. I. Seok, *Nat. Mater.*, 2014, **13**, 897–903.
5 H. Zhou, Q. Chen, G. Li, S. Luo, T. B. Song, H. S. Duan, Z. Hong, J. You, Y. Liu and Y. Yang, *Science*, 2014, **345**, 542–546.
6 N. J. Jeon, J. H. Noh, W. S. Yang, Y. C. Kim, S. Ryu, J. Seo and S. I. Seok, *Nature*, 2015, **517**, 476–480.
7 J. H. Noh, S. H. Im, J. H. Heo, T. N. Mandal and S. I. Seok, *Nano Lett.*, 2013, **13**, 1764–1769.
8 Z.-K. Tan, R. S. Moghaddam, M. L. Lai, P. Docampo, R. Higler, F. Deschler, M. Price, A. Sadhanala, L. M. Pazos, D. Credgington, F. Hanusch, T. Bein, H. J. Snaith and R. H. Friend, *Nat. Nanotechnol.*, 2014, **9**, 687–692.
9 Y.-H. Kim, H. Cho, J. H. Heo, T.-S. Kim, N. Myoung, C.-L. Lee, S. H. Im and T.-W. Lee, *Adv. Mater.*, 2015, **27**, 1248–1254.
10 F. Deschler, M. Price, S. Pathak, L. E. Klintberg, D.-D. Jarausch, R. Higler, S. Hüttner, T. Leijtens, S. D. Stranks, H. J. Snaith, M. Atatüre, R. T. Phillips and R. H. Friend, *J. Phys. Chem. Lett.*, 2014, **5**, 1421–1426.
11 L. Gil-Escrig, G. Longo, A. Pertegas, C. Roldan-Carmona, A. Soriano, M. Sessolo and H. J. Bolink, *Chem. Commun.*, 2015, **51**, 569–571.
12 L. C. Schmidt, A. Pertegás, S. González-Carrero, O. Malinkiewicz, S. Agouram, G. Mínguez Espallargas, H. J. Bolink, R. E. Galian and J. Pérez-Prieto, *J. Am. Chem. Soc.*, 2014, **136**, 850–853.
13 S. Gonzalez-Carrero, R. E. Galian and J. Perez-Prieto, *J. Mater. Chem. A*, 2015, **3**, 9187–9193.
14 F. Zhang, H. Zhong, C. Chen, X.-G. Wu, X. Hu, H. Huang, J. Han, B. Zou and Y. Dong, *ACS Nano*, 2015, **9**, 4533–4542.
15 H. Huang, A. S. Susha, S. V. Kershaw, T. F. Hung and A. L. Rogach, *J. Adv. Sci.*, 2015, **2**, 1500194.
16 F. Zhu, L. Men, Y. Guo, Q. Zhu, U. Bhattacharjee, P. M. Goodwin, J. W. Petrich, E. A. Smith and J. Vela, *ACS Nano*, 2015, **9**, 2948–2959.
17 A. Kojima, M. Ikegami, K. Teshima and T. Miyasaka, *Chem. Lett.*, 2012, **41**, 397–399.
18 M. Zhang, H. Yu, M. Lyu, Q. Wang, J.-H. Yun and L. Wang, *Chem. Commun.*, 2014, **50**, 11727–11730.
19 D. Di, K. P. Musselman, G. Li, A. Sadhanala, Y. Ievskaya, Q. Song, Z.-K. Tan, M. L. Lai, J. L. MacManus-Driscoll, N. C. Greenham and R. H. Friend, *J. Phys. Chem. Lett.*, 2015, **6**, 446–450.
20 G. Li, Z.-K. Tan, D. Di, M. L. Lai, L. Jiang, J. H.-W. Lim, R. H. Friend and N. C. Greenham, *Nano Lett.*, 2015, **15**, 2640–2644.
21 T. Leijtens, G. E. Eperon, S. Pathak, A. Abate, M. M. Lee and H. J. Snaith, *Nat. Commun.*, 2013, **4**, 2885.
22 E. Edri, S. Kirmayer, D. Cahen and G. Hodes, *J. Phys. Chem. Lett.*, 2013, **4**, 897–902.
23 K. G. Stamplecoskie, J. S. Manser and P. V. Kamat, *Energy Environ. Sci.*, 2015, **8**, 208–215.
24 K. Tanaka, T. Takahashi, T. Ban, T. Kondo, K. Uchida and N. Miura, *Solid State Commun.*, 2003, **127**, 619–623.
25 V. D'Innocenzo, A. R. Srimath Kandada, M. De Bastiani, M. Gandini and A. Petrozza, *J. Am. Chem. Soc.*, 2014, **136**, 17730–17733.
26 G. Grancini, S. Marras, M. Prato, C. Giannini, C. Quarti, F. De Angelis, M. De Bastiani, G. E. Eperon, H. J. Snaith, L. Manna and A. Petrozza, *J. Phys. Chem. Lett.*, 2014, **5**, 3836–3842.
27 C. Quarti, G. Grancini, E. Mosconi, P. Bruno, J. M. Ball, M. M. Lee, H. J. Snaith, A. Petrozza and F. D. Angelis, *J. Phys. Chem. Lett.*, 2014, **5**, 279–284.
28 M. De Bastiani, V. D'Innocenzo, S. D. Stranks, H. J. Snaith and A. Petrozza, *APL Mater.*, 2014, **2**, 081509.